Christian Paulsen, Theresa Block, Christopher Benndorf, Oliver Oeckler, Judith Bönnighausen, Oliver Janka and Rainer Pöttgen\*

# Squares of gold atoms and linear infinite chains of Cd atoms as building units in the intermetallic phases $REAu_4Cd_2$ (RE=La-Nd, Sm) with YbAl<sub>4</sub>Mo<sub>2</sub>-type structure

https://doi.org/10.1515/znb-2019-0153 Received September 17, 2019; accepted October 20, 2019

**Abstract:** The gold-rich intermetallic compounds  $REAu_4Cd_2$  (RE=La-Nd, Sm) were synthesized from the elements in sealed tantalum ampoules. Their characterization by X-ray powder and single crystal data confirmed the tetragonal YbAl $_4$ Mo $_2$  type, space group I4/mmm. The basic building units are  $Au_4$  squares (278 pm Au–Au in  $CeAu_4Cd_2$ ) and infinite linear cadmium chains (275 pm Cd–Cd in  $CeAu_4Cd_2$ ). We exemplarily studied the solid solution  $CeAu_{4+x}Cd_{2-x}$  for x=0-1 up to  $CeAu_5Cd$ . Electron diffraction patterns on a  $CeAu_5Cd$  sample confirm the single crystal data. They give no hint for complete gold-cadmium ordering. Temperature-dependent magnetic susceptibility measurements of  $CeAu_4Cd_2$ ,  $CeAu_5Cd$ ,  $PrAu_4Cd_2$  and  $NdAu_4Cd_2$  show stable trivalent rare earth ions and give no hint for magnetic ordering above 3 K.

**Keywords:** cadmium; crystal structure; gold; intermetallics; rare earth.

**Dedicated to:** Professor Arndt Simon on the occasion of his  $80^{\text{th}}$  birthday.

#### 1 Introduction

The structures of intermetallic compounds can be described by the condensation of the different coordination polyhedra or via pronounced substructures of the individual components. This can nicely be illustrated for the YbAl<sub>4</sub>Mo<sub>2</sub> type (Fig. 1) [1]. The molybdenum atoms form infinite linear chains which extend along [001] with

Mo–Mo distances of 266 pm, indicating bonding interactions, since the distances are even slightly shorter than in *bcc* molybdenum (273 pm Mo–Mo) [2]. The same holds true for the aluminum substructure. Al $_4$  squares with Al–Al distances of 265 pm are condensed via Al–Al distances of 284 pm, both again shorter than in *fcc* aluminum (286 pm) [2]. Alternatively, one can describe the YbAl $_4$ Mo $_2$  structure through polyhedra. The ytterbium atoms fill larger cages within the aluminum substructure, and these Yb@Al $_{12}$  polyhedra are condensed with the Mo@Al $_8$ Mo $_2$  polyhedra via common edges.

So far, the Pearson data base [3] lists 62 entries for the YbAl<sub>4</sub>Mo<sub>2</sub> type, space group I4/mmm, Pearson symbol tI14 and Wyckoff sequence hda. Besides the series of rare earth (RE) aluminum compounds  $REAl_4Mo_2$  [1, 4], also the aluminum phases YbCu<sub>5.1</sub>Al<sub>0.9</sub> [5], YbCu<sub>5.12</sub>Al<sub>0.88</sub> [6] and UCu<sub>5</sub>Al [7, 8] have been reported. Here the Cu atoms occupy the Al sites, while the Mo site is mixed occupied by Cu and Al. The higher congener gallium forms the series  $REGa_4Ti_2$  [9–14] and  $REGa_4V_2$  [15–18]. Especially HfGa<sub>4</sub>V<sub>2</sub> and ScGa<sub>4</sub>V<sub>2</sub> of the latter series have intensively been studied with respect to their superconducting properties and elastic anisotropy [17, 18].

The infinite chains in this structure type can also be formed by magnesium, zinc, cadmium, and indium atoms. The four series  $REAg_{4+x}Mg_{2-x}$  [19–21],  $AAu_{4+x}Zn_{2-x}$  (A=Ca, RE) [22, 23],  $AAu_{4+x}Cd_{2-x}$  (A=Ca, Sr, RE) [24], and  $AAu_{4+x}In_{2-x}$  (A=Sr, Eu) [25–27] are known. A common feature of all these phases is their ability to form solid solutions on the 4d Wyckoff sites, i.e. within the linear chains. So far, only few property studies have been performed. Compounds  $REAu_4Zn_2$  with RE=Ce, Pr, Nd show Curie-Weiss behaviour without magnetic ordering down to 2.5 K [22]. The rare earth atoms thus show a stable trivalent ground state. This is different in  $EuAu_4Cd_2$  [24], which, according to magnetic susceptibility data and  $^{151}Eu$  Mößbauer spectra, shows stable divalent europium and ferromagnetic ordering below  $T_C=16.3$  K.

A further example is the intermetallic compound  $CeCu_{_{4,7}}Mn_{_{1,3}}$  [28] with statistical Cu/Mn occupancy on the 4d site.  $CeCu_{_{4,7}}Mn_{_{1,3}}$  can be considered as just one possible composition, and one can expect at least a small homogeneity range.

<sup>\*</sup>Corresponding author: Rainer Pöttgen, Institut für Anorganische und Analytische Chemie, Universität Münster, Corrensstrasse 30, 48149 Münster, Germany, e-mail: pottgen@uni-muenster.de Christian Paulsen, Theresa Block, Judith Bönnighausen and Oliver Janka: Institut für Anorganische und Analytische Chemie, Universität Münster, Corrensstrasse 30, 48149 Münster, Germany Christopher Benndorf and Oliver Oeckler: Institut für Mineralogie, Kristallographie und Materialwissenschaft, Universität Leipzig, Scharnhorststraße 20, D-04275 Leipzig, Germany

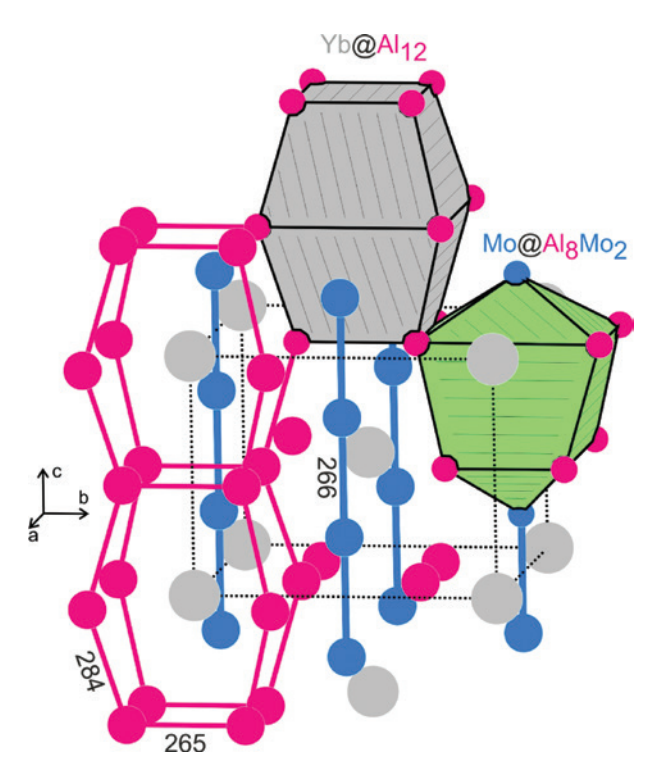


**Fig. 1:** The crystal structure of YbAl<sub>4</sub>Mo<sub>2</sub> [1]. Ytterbium, molybdenum and aluminum atoms are drawn as medium grey, blue and magenta circles, respectively. The infinite molybdenum chains, the aluminum substructure and the Yb@Al<sub>12</sub> and Mo@Al<sub>8</sub>Mo<sub>2</sub> polyhedra are emphasized.

The different coloring variants [29, 30] listed above are summarized in Fig. 2. The distinctly different site occupancies lead to different valence electron counts and pronounced differences in chemical bonding. Most of these phases should consequently be called isopointal [31, 32] rather than isotypic.

An interesting situation concerns those solid solutions where exactly half of the atoms of the linear chains are substituted. A splitting of the 4d site is possible through a *klassengleiche* symmetry reduction of index 2 to space group P4/nmm [33]. Two chemically different site occupancy variants have been discovered. In the solid solution  $\text{LaAg}_{4+x}\text{Mg}_{2-x}$  [19, 20], ordered -Ag-Mg-Ag-Mg-chains occur in  $\text{LaAg}_{5}\text{Mg}$  while the intermediate-valent compound  $\text{Ce}_{2}\text{RuZn}_{4}$  [34–36] shows  $-\text{Ce}^{\text{IV}}-\text{Ru-Ce}^{\text{IV}}-\text{Ru-chains}$  with short  $\text{Ce}^{\text{IV}}-\text{Ru}$  distances of 260 pm, while the other half of the cerium atoms has remained trivalent.

In the course of our phase analytical studies of the *RE-T*-Cd systems (T= electron-rich transition metal) [37], we have extended the  $REAu_4Cd_2$  series including the trivalent rare earths La–Nd and Sm, for which there are also hints for the formation of solid solutions  $REAu_{4+x}Cd_{2-x}$ , that have been studied exemplarily for cerium.

Coloring for the Wyckoff sequence *hda*, space group *I4/mmm* 

2a	4 <i>d</i>	8 <i>h</i>
Yb	Мо	Al
Ce	Zn	Au
La	Mg	Ag
Y	Ti	Ga
Ca	Cd	Au
U	Cu/Al	Cu
Се	Mn/Cu	Cu
Sr	Au/In	Au

Coloring for the Wyckoff sequence *jcba*, space group *P4/nmm* 

2 <i>c</i>	2 <i>b</i>	2a	8 <i>j</i>
Се	Ce	Ru	Zn
La	Mg	Ag	Ag
Се	Cd	Au	Au

Fig. 2: Examples of coloring variants for YbAl<sub>4</sub>Mo<sub>2</sub>-type representatives (space group I4/mmm) and ordered superstructure variants in the *klassengleiche* subgroup P4/nmm.

## 2 Experimental

#### 2.1 Synthesis

Starting materials for the syntheses of the REAu Cd. samples with RE=La-Nd and Sm, were sublimed rare earth metal pieces (Smart Elements, 99.9%), gold drops or gold sheets (Agosi AG, 99.9%) and a cadmium rod (Sigma-Aldrich, 99.999%). The larger moisture sensitive rare earth pieces were cut under dry cyclohexane and stored in Schlenk tubes prior to the reactions. The three elements were then weighed in the ideal atomic ratios (approximate total masses of 250 mg) and arc-welded [38] in tantalum ampoules. The solid solution CeAu, Cd, was studied exemplarily in x = 0.2 steps up to x = 1. Due to the low boiling temperature of cadmium (T=1038 K [39]), an excess of 3 weight-percent cadmium was used for each sample. This compensates approximately for the loss due to film formation at the top lid of the tubes after the annealing sequence.

The sealed tantalum ampoules were subsequently placed in a water-cooled sample chamber [40] of a highfrequency furnace (Hüttinger Elektronik, Freiburg, type TIG 1.5/300) and first rapidly heated to ca. 1473 K. This temperature was kept for 5 min, decreased to 923 K within 10 min and kept for another 4 h, followed by quenching. The temperature was controlled through a radiation pyrometer (Metis MS09, Sensortherm) with an accuracy of ±50 K.

The samples could mechanically be separated from the containers. No reaction with the ampoule material was evident. X-ray powder patterns of these inductively annealed samples showed significantly broadened reflections and by-products, inter alia binary AuCd with CsCltype structure [3]. In order to increase the crystallinity and the phase purity, all samples were subsequently ground to powders, cold-pressed to pellets and annealed in sealed silica tubes in a muffle furnace at 823 K. This annealing step is essential, as it leads to a significantly improved purity of the samples. The product phases are light grey/ golden with some metallic lustre and stable in air.

#### 2.2 X-ray diffraction

The polycrystalline products were characterized through Guinier patterns (Enraf-Nonius FR552 camera, imaging plate detector, Fuji film BAS-1800), which were recorded using  $CuK\alpha_1$  radiation and  $\alpha$ -quartz ( $\alpha$ =491.30, c=540.46 pm) as an internal standard. The tetragonal lattice parameters (Table 1) were deduced from least-squares refinements. Correct indexing was ensured by comparison with calculated patterns using the LAZY PULVERIX routine [41]. As

Table 1: Refined lattice parameters (Guinier powder data) of the intermetallic compounds REAu, Cd, (RE=La-Nd, Sm) and the solid solution  $CeAu_{4+x}Cd_{2-x}$ .

Compound	a (pm)	<i>c</i> (pm)	V (nm³)
LaAu, Cd,	716.73(8)	550.1(1)	0.2826
CeAu <sub>4</sub> Cd <sub>2</sub>	714.6(1)	551.9(1)	0.2818
CeAu <sub>4.2</sub> Cd <sub>1.8</sub>	714.35(7)	550.03(9)	0.2807
CeAu <sub>4.4</sub> Cd <sub>1.6</sub>	714.69(8)	547.9(2)	0.2799
CeAu <sub>4.6</sub> Cd <sub>1.4</sub>	714.58(6)	545.54(7)	0.2786
CeAu <sub>4.8</sub> Cd <sub>1.2</sub>	714.33(9)	544.20(7)	0.2777
CeAu <sub>5.0</sub> Cd <sub>1.0</sub>	714.25(8)	546.13(9)	0.2786
PrAu <sub>4</sub> Cd <sub>2</sub>	712.4(1)	549.5(2)	0.2789
NdAu Cd,	711.8(1)	548.9(2)	0.2781
SmAu <sub>4</sub> Cd <sub>2</sub>	710.7(2)	547.0(2)	0.2763
EuAu <sub>4</sub> Cd <sub>2</sub> [24]	717.0(1)	553.2(2)	0.2844

Standard deviations are given in parentheses.

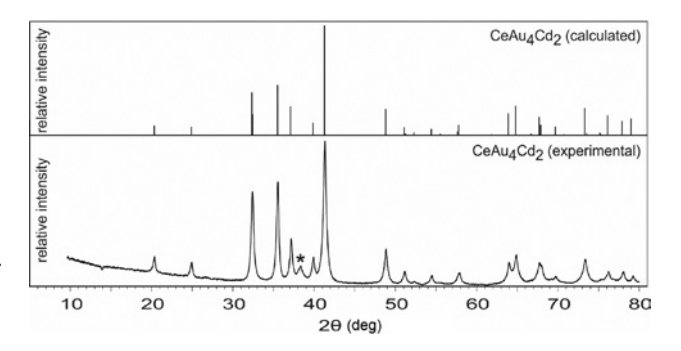


Fig. 3: Experimental and calculated Guinier powder pattern ( $CuK\alpha$ , radiation) of CeAu, Cd2. The asterisk marks a reflection originating from the by-product AuCd with CsCl-type structure.

an example, we present the experimental and simulated CeAu, Cd, powder diagram in Fig. 3.

Single crystal fragments were isolated from the annealed CeAu<sub>4</sub>Cd<sub>2</sub> and CeAu<sub>4</sub>2Cd<sub>18</sub> samples. The blockshaped splinters were glued to quartz fibres using beeswax and their quality was first tested on a Buerger camera (white Mo radiation). Complete intensity data sets were collected by use of a Stoe IPDS-II diffractometer (graphite-monochromatized Mo $K\alpha$  radiation; oscillation mode). Numerical absorption corrections were applied to both data sets. Details of the data collections, the crystallographic parameters and the refinements are summarized in Table 2.

#### 2.3 Structure refinements

The data sets of the crystals with nominal compositions CeAu, Cd, and CeAu, Cd, showed tetragonal body-centred unit cells with 4/mmm Laue symmetry and no further systematic extinctions. Space group I4/mmm was found to be correct, in agreement with previous results on isotypic CaAu Cd. [24]. The atomic parameters of the calcium compound were taken as starting values and the structures were refined with full-matrix least-squares on  $F_0^2$  using the program Jana2006 [42] with anisotropic displacement parameters for all atoms. Separate refinements of the occupancy parameters revealed full occupancies for CeAu, Cd,. The second crystal showed Au/Cd mixing on the 4d site. This mixed occupancy was refined as a least-squares variable in the final cycles and resulted in the composition CeAu<sub>4.67(1)</sub>Cd<sub>1.33(1)</sub> for the investigated crystal. The final difference Fourier syntheses revealed no significant residual peaks. The atomic positions, displacement parameters, and interatomic distances are given in Tables 3 and 4.

CCDC 1953900 (CeAu, Cd,) and 1953960 (CeAu, c7Cd, 33) contain the supplementary crystallographic data for this

Table 2: Crystallographic data and structure refinement of CeAu<sub>4</sub>Cd<sub>2</sub> and CeAu<sub>4.67(1)</sub>Cd<sub>1.33(1)</sub>; YbAl<sub>4</sub>Mo<sub>2</sub> type, space group /4/mmm, Z=2.

Empirical formula	CeAu <sub>4</sub> Cd <sub>2</sub>	CeAu <sub>4.67(1)</sub> Cd <sub>1.33(1)</sub>	
Formula weight, g mol <sup>-1</sup>	1152.8	1209.4	
Lattice parameters (single crystal data)			
a, pm	714.65(11)	714.01(6)	
<i>c</i> , pm	550.86(9)	544.65(5)	
Cell volume, nm <sup>3</sup>	0.2813	0.2777	
Calculated density, g cm <sup>-3</sup>	13.61	14.46	
Crystal size, μm³	$30 \times 35 \times 100$	$20\times30\times165$	
Transm. ratio (min/max)	0.154/0.054	0.164/0.037	
Diffractometer type	IPDS-II (Stoe)	IPDS-II (Stoe)	
Detector distance, mm	70	70	
Exposure time, min	5	5	
$\omega$ range/step width, deg	0-180/1.0	0-180/1.0	
Integr. Param. A/B/EMS	14.0/-1.0/0.030	14.0/4.0/0.010	
Abs. coefficient, mm <sup>-1</sup>	119.0	135.7	
F(000), e	940	981	
$\theta$ range, deg	4.03-33.43	4.04-33.22	
hkl range	$\pm 10, \pm 11, \pm 8$	$\pm 10, \pm 10, \pm 8$	
Total no. reflections	1701	1816	
Independent reflections/R <sub>int</sub>	179/0.0317	179/0.0262	
Refl. with $I > 3 \sigma(I)/R_{\sigma}$	162/0.0070	169/0.0048	
Data/parameters	179/10	179/11	
Goodness-of-fit on F <sup>2</sup>	2.50	1.82	
$R1/wR2$ for $I > 3 \sigma(I)$	0.0288/0.0623	0.0200/0.0435	
R1/wR2 for all data	0.0320/0.0628	0.0217/0.0439	
Extinction coefficient	520(30)	187(11)	
Largest diff. peak/hole, e Å-3	3.77/-2.18	1.88/-1.79	

Table 3: Atomic positions and isotropic displacement parameters (pm²) of CeAu<sub>4</sub>Cd<sub>2</sub> and CeAu<sub>4.67(1)</sub>Cd<sub>1.33(1)</sub> (YbAl<sub>4</sub>Mo<sub>2</sub> type, space group I4/mmm, Z=2).

Atom	Wyck. site	х	у	Z	<b>U</b> <sub>11</sub>	U <sub>33</sub>	<b>U</b> <sub>12</sub>	U <sub>eq</sub>
CeAu, Cd,								
Ce	2 <i>a</i>	0	0	0	140(5)	157(8)	0	146(4)
Au	8 <i>h</i>	0.30555(6)	X	0	140(3)	181(4)	7(2)	153(2)
Cd	4 <i>d</i>	0	1/2	1/4	157(4)	131(7)	0	148(3)
CeAu <sub>4.67(1)</sub> Cd <sub>1.33(1)</sub>								
Ce	2 <i>a</i>	0	0	0	138(8)	169(5)	0	148(2)
Au1	8 <i>h</i>	0.30546(4)	X	0	139(2)	183(2)	8(1)	153(1)
0.67(1) Cd/0.33(1) Au2	4 <i>d</i>	0	1/2	1/4	167(3)	136(4)	0	157(2)

The equivalent isotropic displacement parameter  $U_{eq}$  is defined as  $U_{eq} = 1/3$  ( $U_{11} + U_{22} + U_{33}$ ) (pm²).  $U_{22} = U_{11}$ ,  $U_{13} = U_{23} = 0$ . Standard deviations are given in parentheses.

paper. These data can be obtained free of charge from The Cambridge Crystallographic Data Centre via www.ccdc. cam.ac.uk/data\_request/cif.

#### 2.4 EDX data

The crystals of  $CeAu_4Cd_2$  and  $CeAu_{4.67(1)}Cd_{1.33(1)}$  studied on the single crystal diffractometer were analyzed by EDX

in variable pressure mode (60 Pa) using a Zeiss EVO® MA10 scanning electron microscope with CeO<sub>2</sub>, Au and Cd as standards. Each crystal was analyzed at 10 points. The averaged values of  $13\pm2$  at% Ce:  $58\pm2$  at% Au:  $29\pm2$  at% Cd for the CeAu<sub>4</sub>Cd<sub>2</sub> (14.3: 57.1:28.6) and  $14 \pm 2$  at% Ce:  $66 \pm 2$ at% Au:  $20\pm2$  at% Cd for the  $CeAu_{4.67}Cd_{1.33}$  (14.3:66.7:19.0) crystal confirmed the X-ray data. No impurity elements (especially with respect to the tantalum of the containers) were observed.

Table 4: Interatomic distances (pm) for CeAu<sub>4</sub>Cd<sub>2</sub> and CeAu<sub>4.67(1)</sub>Cd<sub>1.33(1)</sub>.

CeAu <sub>4</sub> Cd <sub>2</sub>					CeAu <sub>4.67(1)</sub> Cd <sub>1.33(1)</sub>			
Ce:	4	Au	308.8	Ce:	4	Au	308.4	
	8	Au	338.4		8	Au	335.8	
	8	Cd	382.9		8	Μ	382.1	
Au:	2	Au	277.9	Au:	2	Au	277.8	
	4	Cd	293.2		4	М	292.2	
	2	Au	297.4		2	Au	294.5	
	1	Ce	308.8		1	Ce	308.4	
	2	Ce	338.4		2	Ce	335.8	
Cd:	2	Cd	275.4	М:	2	М	272.3	
	8	Au	293.2		8	Au	292.2	
	4	Ce	382.9		4	Ce	382.1	

Standard deviations are equal or smaller than 0.1 pm. All distances of the first coordination spheres are listed. Note that the M site shows a mixed occupancy of 67(1)% Cd and 33(1)% Au.

#### 2.5 Electron microscopy

CeAu<sub>c</sub>Cd was investigated by using a Phillips CM-200 STEM transmission electron microscope (200 kV, point resolution 0.23 nm) equipped with a super twin objective lens and an EDAX EDX system. A small piece of sintered CeAu, Cd was cooled down using liquid nitrogen in a steel mortar. The sample was carefully crushed into small particles to prevent mechanical damage of the crystals. The sample was suspended in ethanol, transferred to a carbon-coated copper grid (Plano) and investigated using a double-tilt low-background sample holder (Gatan). The chemical composition of the investigated crystal (Fig. 4) was measured by EDX analyses at several areas of the investigated crystal. Selected-area electron diffraction

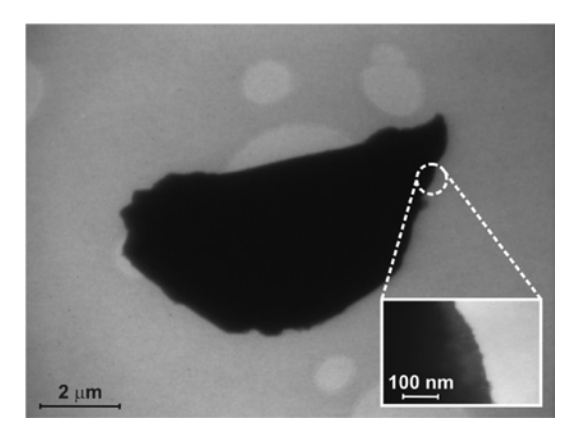


Fig. 4: TEM bright-field image of the investigated CeAu, Cd crystal. The area used to obtain SAED patterns is emphasized by a white circle and visualized by an enlarged view.

(SAED) patterns were simulated using the JEMS software package [43, 44].

#### 2.6 Physical property studies

Polycrystalline powders of CeAu, Cd., PrAu, Cd., NdAu, Cd. as well as CeAu, Cd were packed in polyethylene (PE) capsules and attached to the sample holder rod of a Vibrating Sample Magnetometer unit (VSM) for measuring the magnetization M(T,H) in a Quantum Design Physical Property Measurement System (PPMS). The samples were investigated in the temperature range of 2.5-300 K and with applied magnetic fields up to 80 kOe  $(1 \text{ kOe} = 7.96 \times 10^4 \text{ A m}^{-1}).$ 

### 3 Crystal chemistry

Our studies in the gold-rich parts of the RE-Au-Cd systems with the early rare earth elements revealed the YbAl, Mo,type phases  $REAu_{k}Cd_{k}$  with RE=La-Nd and Sm. The crystal chemical details of the YbAl, Mo, type have repeatedly been discussed [13, 19, 20, 22]. In the following discussion we therefore mainly focus on the structural details that are directly associated with the formation of the solid solution CeAu, Cd, Cd,

Figure 5 shows a projection of the CeAu, Cd, structure onto the xy plane. The gold atoms build a substructure with two different Au, cages. The larger cerium atoms fill the middle of one of these cages (Fig. 5, left), while pairs of cadmium atoms fill the second one (Fig. 5, middle). These  $Au_{12}$  cages are condensed in c direction via common gold rectangles. This leads to infinite cadmium chains with Cd-Cd distances of 275 pm, which are even shorter than in hcp cadmium (6  $\times$  298 and 6  $\times$  329 pm) [2]. The rows of these condensed polyhedra are arranged in form of a tetragonal rod packing [45-47].

The gold substructure shows Au-Au distances of 278 and 297 pm, close to the Au-Au distances in fcc gold (288 pm [2]). The cadmium chains bind to the gold substructure via Au-Cd contacts with 293 pm Au-Cd, significantly longer than the sum of the covalent radii [39] for Au+Cd of 275 pm, indicating weaker Au-Cd bonding.

Keeping the Pauling electronegativities [39] in mind (1.12 for Ce, 2.54 for Au and 1.69 for Cd), we can ascribe auride character to CeAu, Cd., similar to isotypic CaAu, Cd., [24]. A Bader charge analysis of the latter compound revealed +1.98 for Ca, +0.43 for Cd and -0.71 for Au. The other gold-containing YbAl, Mo,-type phases show the same electronic fingerprint.

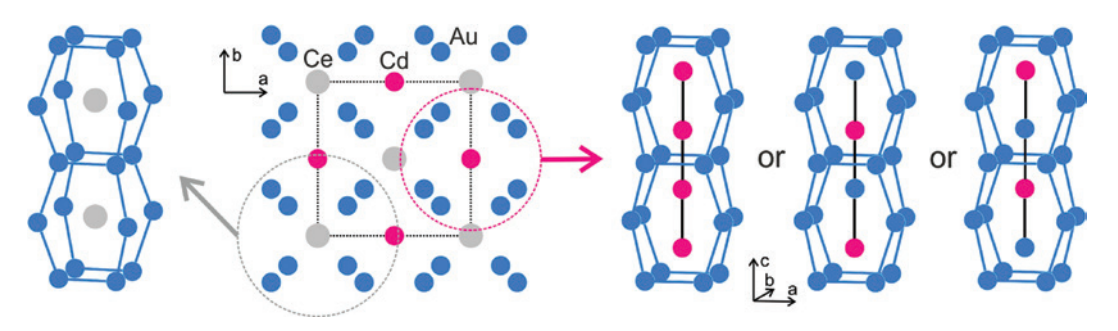
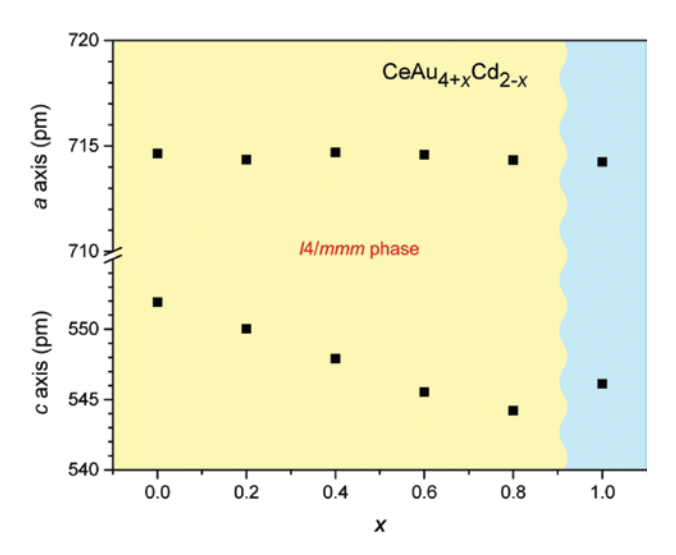


Fig. 5: Projection of the  $CeAu_4Cd_2$  structure along [001]. Cerium, gold and cadmium atoms are drawn as medium grey, blue and magenta circles, respectively. The coordination of the cerium respectively cadmium atoms is outlined at the left- and right-hand part of the unit cell along with two ordering models for alternating Au/Cd occupancy within the linear chains for the gold-rich compound  $CeAu_cCd$ .

Detailed phase analytical work revealed the formation of extended solid solutions for several of the YbAl, Mo,type phases, resulting from continuous substitution of the chain atoms on Wyckoff position 4d by the transition metal [19–27]. This is also the case for CeAu, Cd, reported herein. We observe the complete solid solution CeAu, Cd, up to x=1. The lattice parameters of the CeAu<sub>xx</sub>Cd<sub>xx</sub> samples are summarized in Table 1 and plotted as a function of the x value in Fig. 6. The lattice parameter a is approximately unaffected by the substitution while c decreases with increasing gold content, since cadmium atoms (covalent radius of 141 pm [39]) are substituted by smaller gold atoms (covalent radius 134 pm [39]). Whereas the decrease of c is almost linear for the solid solution EuAu, Cd, [24] up to EuAu<sub> $\epsilon$ </sub>Cd, for the x=1 sample of the solid solution  $CeAu_{h,v}Cd_{2-v}$  we observe a small recovery for the c parameter, as it has also been observed within the solid solution LaAg, Mg, [19], where it has been associated



**Fig. 6:** Course of the lattice parameters a and c of the solid solution  $CeAu_{A+X}Cd_{2-X}$ . 1:1 Gold-cadmium ordering within the chains is possible around x=1 (blue shaded region). For details see text.

with superstructure formation. In an ordered model for x=1 (i.e. LaAg, Mg or CeAu, Cd) one observes alternating chains -Ag-Mg-Ag-Mg- or -Au-Cd-Au-Cd- extending in *c* direction. The complete ordering leads to a symmetry reduction. A single crystal structure refinement of LaAg, Mg [20] clearly manifested space group P4/nmm, a klassengleiche subgroup of index 2 of I4/mmm. The splitting of the 4d site into two two-fold sites allows for the -Ag-Mg-Ag-Mg- ordering [19]. The corresponding group-subgroup scheme for the pair LaAg, Mg, (I4/mmm)/ LaAg<sub>r</sub>Mg (P4/nmm) has been described in detail in [19, 20]. It is similar to the pair CeAu<sub>e</sub>Cd<sub>2</sub> (I4/mmm)/Ce<sub>2</sub>RuZn<sub>4</sub> (P4/nmm) [22]. Ce<sub>2</sub>RuZn<sub>4</sub> is a static mixed-valence cerium compound with an ordering of Ce<sup>IV</sup> and Ru on the linear chain. In view of the completely different bonding pattern, LaAg<sub>s</sub>Mg and Ce<sub>3</sub>RuZn<sub>4</sub> are only isopointal [31, 32].

Thus, the occurrence of primitive (superstructure) reflections indicates the ordering within the chains. The  $CeAu_{4,67(1)}Cd_{1,33(1)}$  crystal still shows a body-centered lattice without evidence for Au/Cd long-range ordering. Unfortunately, the annealed CeAu<sub>c</sub>Cd sample prepared in this work was essentially polycrystalline and it was not possible to select sufficiently large crystals for a diffraction study. Therefore, we have analyzed the Guinier powder pattern (Fig. 7) in more detail. Besides the experimental pattern we present three different calculated powder patterns, all with the same lattice parameters: (i) the subcell structure of CeAu, Cd, in space group I4/mmm, (ii) the subcell structure of CeAu<sub>E</sub>Cd in space group I4/mmm with a statistical 50% Au and 50% Cd occupancy on Wyckoff site 4d, and (iii) the fully ordered model for CeAu, Cd in the primitive subgroup P4/nmm.

The substantial population of the chain with gold atoms leads to an increase of the intensity of the 110 reflection at  $2\theta = 17.55^{\circ}$  (green arrow in Fig. 7). However, the weak superstructure reflections (red arrows in Fig. 7) that occur in the fully ordered P4/nmm model are not visible in our experimental powder pattern. As emphasized at

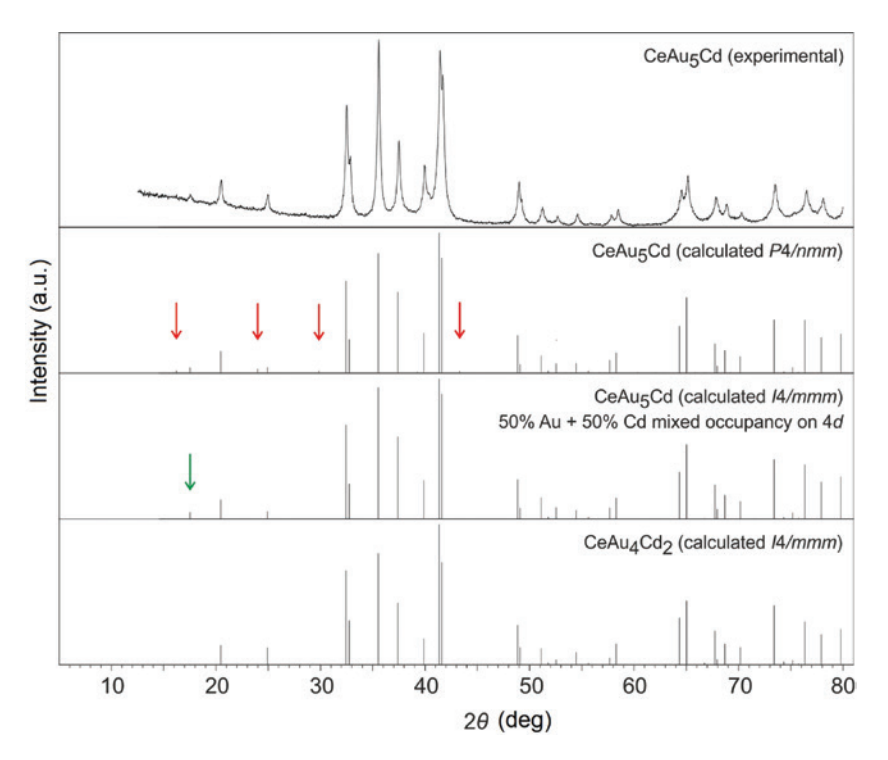


Fig. 7: The experimental Guinier powder pattern ( $CuK\alpha$ , radiation) of  $CeAu_{\varsigma}Cd$  (top) along with different simulated powder patterns. Relevant reflections indicating Au/Cd ordering are highlighted by red and green arrows. For details see text.

the right-hand part of Fig. 4, adjacent fully ordered (!) chains can be shifted by half the c axis, avoiding longrange ordering between the chains. We have thus studied our compound CeAu<sub>s</sub>Cd by electron diffraction (vide infra) in order to get more detailed information on the gold/ cadmium ordering within and between the chains.

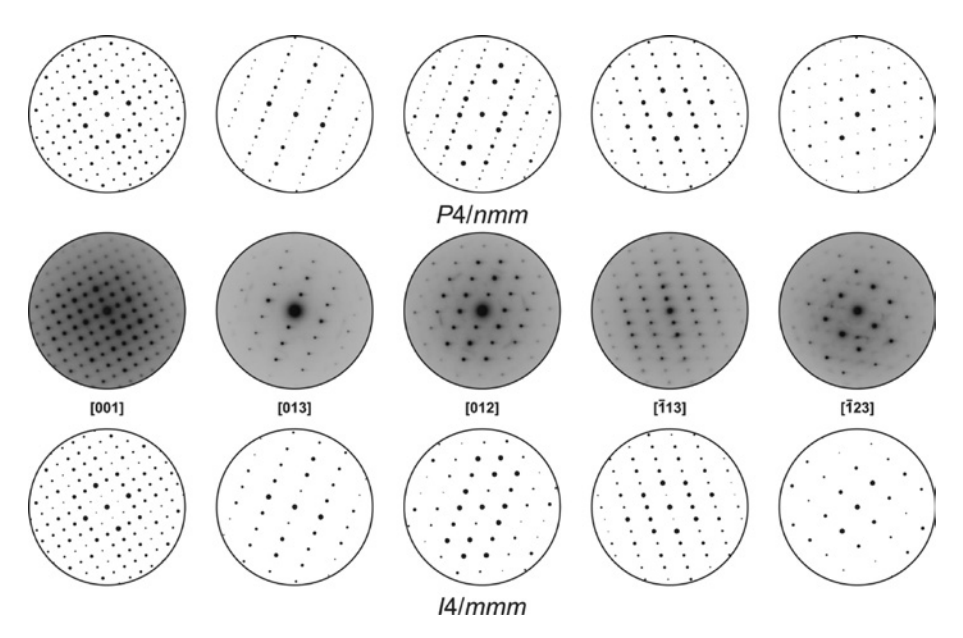
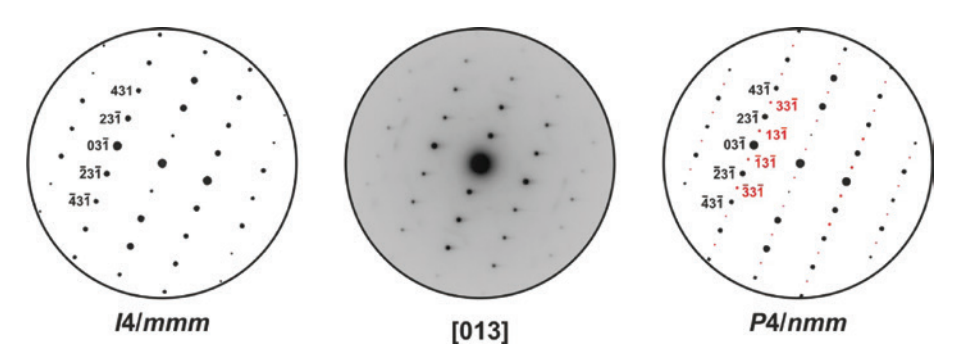
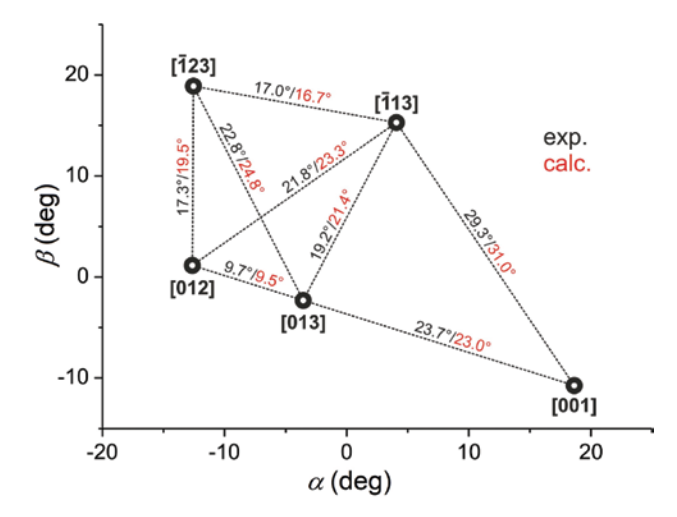


Fig. 8: Experimental (middle) and simulated SAED patterns of the investigated CeAu, Cd crystal obtained along different zone axes. The simulations with kinematic intensities were generated on the basis of the structure models in space groups P4/nmm (top, LaAg, Mg type) and 14/mmm (bottom, YbAl, Mo, type), respectively. Systematic extinction of reflections according to an I centered lattice are observed for the diffraction patterns along [013], [012] and [123]. Diffuse intensity in the SAED patterns is due to poor crystal quality and pronounced intergrowth.



**Fig. 9:** Comparison of the experimental SEAD pattern recorded along [013] and simulated ones (left: l4/mmm; right: P4/nmm). Systematic extinction is observed for reflections (depicted in red) fulfilling  $h+k+l\neq 2n$ , compatible with l centering.

Finally we need to mention that Au/Cd ordering within the chains is also possible in other subgroups. A first possibility is a translationengleiche symmetry reduction to space group  $I\overline{4}m2$ . Refinement of the CeAu, 67(1) Cd, 33(1) data in this space group revealed the same degree of Au/Cd mixing on both twofold sites and 50/50 twin domains, indicating that  $I\overline{4}m2$  is not the correct space group for the investigated crystal. Besides P4/nmm, also P4/mmc is a klassengleiche subgroup. In view of the missing primitive reflections, also space group P4<sub>2</sub>/mmc is not correct. An orthorhombic subgroup along with twinning would also be possible; however, our single crystal data gave no hint for this alternative. Keeping the precise single crystal data of LaAg<sub>2</sub>Mg [20] and Ce<sub>2</sub>RuZn<sub>4</sub> [34–36] and the close structural relationship of magnesium and cadmium intermetallics [37, 48] in mind, the subgroup P4/nmm is the most probable one for the ordering within the chains.



**Fig. 10:** Goniometer positions of the obtained SAED patterns along with experimental (black font) and calculated (red font) tilt angles between the zone axes.

# 4 Electron-microscopic characterization of CeAu<sub>s</sub>Mg

Since superstructure reflections cannot be expected to be detectable in powder X-ray diffraction patterns due to their low relative intensity, the differentiation of the possible space group symmetries I4/mmm (YbAl<sub>4</sub>Mo<sub>2</sub> type) and P4/nmm (LaAg<sub>5</sub>Mg type) was performed by analysis of SAED patterns (Figs. 8–10). The correct space group could be determined by SAED diagrams along [013], [012] and [123] for which systematic extinction according to I centering was observed suggesting mixed Au/Cd occupancy on the 4d site. Investigation of several crystals confirmed this observation. Additionally, results of a TEM-EDX analysis of the investigated crystal are in excellent agreement with the expected composition of CeAu<sub>5</sub>Cd (Ce:  $14\pm1$  at%, Au:  $11\pm1$  at%, Cd:  $15\pm1$  at%, 5 points measured).

# 5 Magnetic properties

CeAu, Cd, CeAu, Cd, PrAu, Cd, and NdAu, Cd, were investigated by magnetic susceptibility measurements at an applied external field of 10 kOe using a zero-field-cooled routine. The  $\chi$  and  $\chi^{-1}$  data of the cerium compounds is exemplarily shown in Figs. 11 and 12, top panel. A fit of the  $\chi^{-1}$  data in the region above T = 50 K using the modified Curie-Weiss law revealed effective magnetic moments of  $\mu_{\rm eff}$  = 2.49(1)  $\mu_{\rm B}$  per Ce atom for CeAu, Cd, and  $\mu_{\rm eff}$  = 2.54(1)  $\mu_{\rm B}$ per Ce atom for CeAu<sub>s</sub>Cd. The effective magnetic moments match the theoretical value for a free Ce<sup>3+</sup>ion ( $\mu_{theo}$  = 2.54  $\mu_{\rm B}$ ). The Weiss constants are  $\theta_n = +8.0(5)$  K (CeAu<sub>4</sub>Cd<sub>2</sub>) and  $\theta_{\rm n}$  = -8.4(5) K (CeAu<sub>5</sub>Cd), suggesting ferromagnetic interactions in the paramagnetic temperature region in the case of CeAu, Cd., while antiferromagnetic interactions are deduced for CeAu, Cd. The temperature independent contributions are  $\chi_0(\text{CeAu}_{\alpha}\text{Cd}_{\gamma}) = -4.44(5) \times 10^{-4} \text{ emu mol}^{-1} \text{ and}$ 

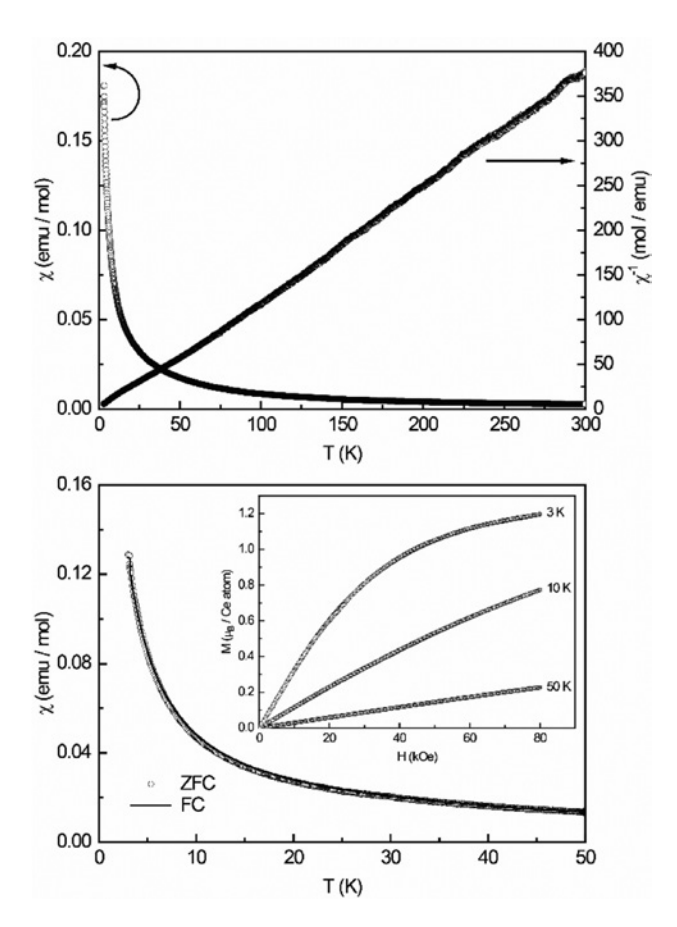


Fig. 11: Magnetic properties of CeAu, Cd,: (top) temperature dependence of the magnetic susceptibility  $\chi$  and its reciprocal  $\chi^{-1}$ measured with an applied magnetic field of 10 kOe; (bottom) magnetic susceptibility in zero-field (ZFC) and field-cooled (FC) mode at 100 Oe; (inset) magnetization isotherms recorded at T=3, 10, and 50 K.

 $\chi_0(\text{CeAu}_s\text{Cd}) = -1.25(3) \times 10^{-4} \text{ emu mol}^{-1}$ . To obtain more information about possible ordering phenomena, lowfield measurements were performed in zero-field and fieldcooled mode (ZFC/FC), the data is shown in the bottom panels of Figs. 11 and 12. No bifurcation between the ZFC and FC curve and no magnetic ordering was observed down to 3.0 K. The insets in Figs. 11 and 12 (bottom panels) display the magnetization isotherms measured at T=3, 10, and 50 K. The 10 and 50 K isotherms display a linear field dependency of the magnetization, as expected for a paramagnetic material. The 3 K isotherm exhibits curvatures along with the onset of saturation at high fields. The magnetizations at 3 K and 80 kOe reach  $\mu_{\rm sat}$  = 1.20(2)  $\mu_{\rm B}$ per Ce atom (CeAu<sub>4</sub>Cd<sub>2</sub>) and  $\mu_{sat}$  = 1.04(2)  $\mu_{R}$  per Ce atom (CeAu<sub>s</sub>Cd), which is drastically below the expected saturation magnetization of 2.14  $\mu_{\scriptscriptstyle B}$  per Ce atom according to  $g_1 \times J$ , however in line with that of several other intermetallic cerium compounds [49, 50].

Also PrAu, Cd, and NdAu, Cd, exhibit no magnetic ordering down to T = 2.5 K. The effective magnetic moments are in

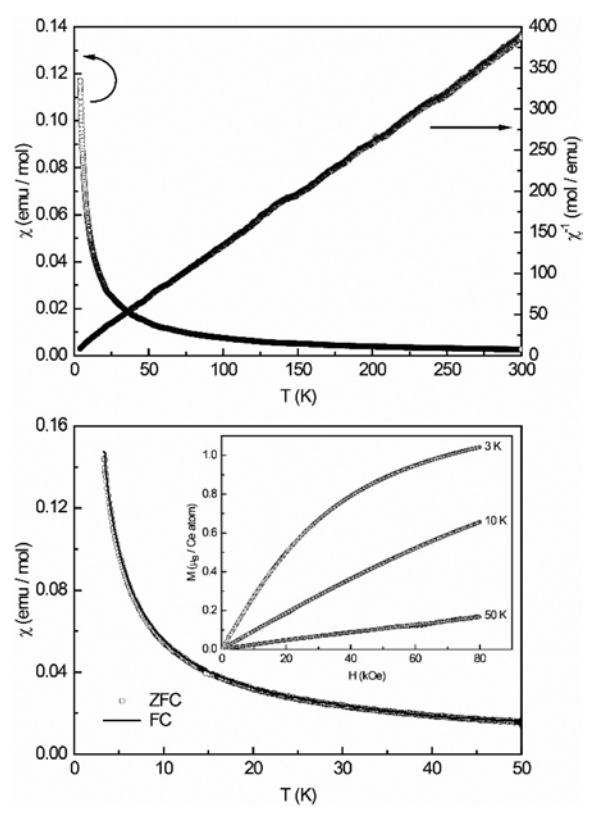


Fig. 12: Magnetic properties of CeAu, Cd: (top) temperature dependence of the magnetic susceptibility  $\chi$  and its reciprocal  $\chi^{-1}$  measured with an applied magnetic field of 10 kOe; (bottom) magnetic susceptibility in zero-field (ZFC) and field-cooled (FC) mode at 100 Oe; (inset) magnetization isotherms recorded at T=3, 10, and 50 K.

line with the calculated ones, indicating purely trivalent oxidation states  $(\mu_{eff}(PrAu_{a}Cd_{2}) = 3.75(1) \mu_{R}; \mu_{calc}(Pr^{3+}) = 3.58 \mu_{R};$  $\mu_{\text{eff}}(NdAu_{\mu}Cd_{\nu}) = 3.55(1) \ \mu_{\text{R}}; \ \mu_{\text{calc}}(Nd^{3+}) = 3.62 \ \mu_{\text{R}}).$  The Weiss constants ( $\theta_p(PrAu_{\alpha}Cd_{\gamma}) = -1.5(1) \text{ K}; \theta_p(NdAu_{\alpha}Cd_{\gamma}) = -1.1(1) \text{ K}$ ) are small but negative, indicating antiferromagnetic interactions in the paramagnetic temperature regime. Finally, the magnetizations at T=3 K and 80 kOe are  $\mu_{\text{sat}}(\text{PrAu}_4\text{Cd}_2) = 1.96(1) \ \mu_{\text{B}} \ \text{and} \ \mu_{\text{sat}}(\text{NdAu}_4\text{Cd}_2) = 1.88(1) \ \mu_{\text{B}},$ which are below the theoretical values of  $\mu_{\text{sat,calc}}(Pr^{3+}) = 3.20 \,\mu_{\text{B}}$ and  $\mu_{\text{sat.calc}}(\text{Nd}^{3+}) = 3.27 \,\mu_{\text{B}}$ , a consequence of anisotropy and the polycrystalline character of the samples.

Acknowledgements: We thank Dipl.-Ing. U. Ch. Rodewald for the single crystal data collections.

#### References

- [1] M. L. Fornasini, A. Palenzona, J. Less-Common Met. 1976, 45, 137.
- [2] J. Donohue, The Structures of the Elements, Wiley, New York, 1974.

- [3] P. Villars, K. Cenzual, Pearson's Crystal Data: Crystal Structure Database for Inorganic Compounds (release 2018/19), ASM International®, Materials Park, Ohio (USA), 2018.
- [4] Y. N. Hryn, P. Rogl, Visn. L'viv Derzh. Univ., Ser. Khim. 1986, 27, 38.
- [5] B. M. Stel'makhovych, Y. B. Kuz'ma, V. S. Babyzhet'sky, J. Alloys Compd. 1993, 190, 161.
- [6] B. M. Stel'makhovych, Y. B. Kuz'ma, L. G. Akselrud, Russ. Metall. 1993, 1, 173.
- [7] R. Troć, V. H. Tran, M. Wołcyrz, G. André, F. Bourée, J. Magn. Magn. Mater. 1998, 190, 251.
- [8] Y. Verbovytskyy, A. P. Gonçalves, Intermetallics 2013, 33, 16.
- [9] Y. Grin, I. S. Gavrilenko, V. Y. Markiv, Y. P. Yarmolyuk, Dopov. Akad. Nauk Ukr. RSR, Ser. A 1980, 73.
- [10] V. Y. Markiv, T. G. Zhunkivska, N. M. Velyavina, O. O. Lisenko, Dopov. Akad. Nauk Ukr. RSR, Ser. A 1983, 81.
- [11] K. Gosh, S. Ramakrishnan, G. Chandra, J. Magn. Magn. Mater. 1993, 119, L5.
- [12] H. Abe, K. Yoshii, H. Kitazawa, J. Phys. Soc. Jpn. 2001, 70, 3042.
- [13] S. F. Matar, R. Pöttgen, Z. Naturforsch. 2013, 68b, 23.
- [14] A. Zelinskiy, R. Gladyshevskii, Visn. L'viv Derzh. Univ., Ser. Khim. 2016, 57, 70.
- [15] V. Y. Markiv, Dopov. Akad. Nauk Ukr. RSR, Ser. A 1981, 86.
- [16] Y. Verbovytskyy, J. Alloys Compd. 2016, 666, 440.
- [17] P. P. Ferreira, F. B. Santos, A. J. S. Machado, H. M. Petrilli, L. T. F. Eleno, Phys. Rev. B 2018, 98, 045126.
- [18] P. P. Ferreira, T. T. Dorini, F. B. Santos, A. J. S. Machado, L. T. F. Eleno, Materialia 2018, 4, 529.
- [19] S. De Negri, P. Solokha, V. Pavlyuk, A. Saccone, Intermetallics 2011, 19, 671.
- [20] P. Solokha, S. De Negri, V. Pavlyuk, A. Saccone, G. Fadda, Eur. J. Inorg. Chem. 2012, 4811.
- [21] Y. Verbovytskyy, A. P. Gonçalves, Solid State Sci. 2015, 40, 84.
- [22] B. Gerke, O. Niehaus, R.-D. Hoffmann, Z. Anorg. Allg. Chem. 2013, 639, 2575.
- [23] T. Mishra, Q. Lin, J. D. Corbett, J. Solid State Chem. 2014, 218,
- [24] F. Tappe, S. F. Matar, C. Schwickert, F. Winter, B. Gerke, R. Pöttgen, Monatsh. Chem. 2013, 144, 751.
- [25] I. Muts, S. F. Matar, U. Ch. Rodewald, V. I. Zaremba, R. Pöttgen, Z. Naturforsch. 2011, 66b, 993.
- [26] S. Steinberg, N. Card, A.-V. Mudring, Inorg. Chem. 2015, 54, 8187.

- [27] I. Bigun, S. Steinberg, V. Smetana, Ya. Mudryk, Ya. Kalychak, L. Havela, V. Pecharsky, A.-V. Mudring, Chem. Mater. 2017, 29, 2599.
- [28] P. Manfrinetti, M. L. Fornasini, D. Mazzone, S. K. Dhar, R. Kulkarni, J. Alloys Compd. 2004, 379, 64.
- [29] G. J. Miller, Eur. J. Inorg. Chem. 1998, 1998, 523.
- [30] T.-S. You, M.-K. Han, G. J. Miller, Inorg. Chim. Acta 2008, 361,
- [31] E. Parthé, L. M. Gelato, Acta Crystallogr. A 1984, 40, 169.
- [32] L. M. Gelato, E. Parthé, J. Appl. Crystallogr. 1987, 20, 139.
- [33] U. Müller in International Tables for Crystallography, Vol. A1, Symmetry Relations Between Space Groups (Eds.: H. Wondratschek, U. Müller), 2nd edition, John Wiley & sons, Ltd, Chichester, 2010, pp. 44-56.
- [34] R. Mishra, W. Hermes, U. Ch. Rodewald, R.-D. Hoffmann, R. Pöttgen, Z. Anorg. Allg. Chem. 2008, 634, 470.
- [35] V. Eyert, E.-W. Scheidt, W. Scherer, W. Hermes, R. Pöttgen, Phys. Rev. B 2008, 78, 214420.
- [36] S. Hartwig, K. Prokeš, T. Hansen, C. Ritter, B. Gerke, R. Pöttgen, J. A. Mydosh, T. Förster, Phys. Rev. B 2015, 92, 024420.
- [37] F. Tappe, R. Pöttgen, Rev. Inorg. Chem. 2011, 31, 5.
- [38] R. Pöttgen, Th. Gulden, A. Simon, GIT Labor-Fachzeitschrift 1999, 43, 133.
- [39] J. Emsley, The Elements, Oxford University Press, Oxford, 1999.
- [40] R. Pöttgen, A. Lang, R.-D. Hoffmann, B. Künnen, G. Kotzyba, R. Müllmann, B. D. Mosel, C. Rosenhahn, Z. Kristallogr. 1999, 214,
- [41] K. Yvon, W. Jeitschko, E. Parthé, J. Appl. Crystallogr. 1977, 10, 73.
- [42] V. Petříček, M. Dušek, L. Palatinus, Z. Kristallogr. 2014, 229, 345.
- [43] P. A. Stadelmann, Ultramicroscopy 1987, 21, 131.
- [44] P. A. Stadelmann, JEMS (version 4.4631U), Saas-Fee (Switzerland) 2016. http://www.jems-saas.ch/Home/jemsWebSite/ jems.html.
- [45] M. O'Keeffe, S. Andersson, Acta Crystallogr. 1977, A33, 914.
- [46] S. Lidin, M. Jacob, S. Andersson, J. Solid State Chem. 1995, 114,
- [47] N. L. Rosi, J. Kim, M. Eddaoudi, B. Chen, M. O'Keeffe, O. M. Yaghi, J. Am. Chem. Soc. 2005, 127, 1504.
- U. Ch. Rodewald, B. Chevalier, R. Pöttgen, J. Solid State Chem. 2007, 180, 1720.
- [49] R. Pöttgen, B. Chevalier, Z. Naturforsch. 2015, 70b, 289.
- [50] O. Janka, O. Niehaus, R. Pöttgen, B. Chevalier, Z. Naturforsch. 2016, 71b, 737.